CHAPTER III
SILVER NANOPARTICLE-EMBEDDED POLY(VINYL PYRROLIDONE) HYDROGEL DRESSING: GAMMA-RAY SYNTHESIS AND BIOLOGICAL EVALUATION

3.1 Abstract

Silver nanoparticle (nAg)-embedded poly(vinyl pyrrolidone) (PVP) hydrogels, to be used as antibacterial wound dressings, were prepared by gamma irradiation at various doses: 25, 35 and 45 kGy. The formation and characteristics of the silver nanoparticles were investigated with a UV-Visible spectrophotometer, transmission electron microscopy, and scanning electron microscopy combined with energy-dispersive X-ray. The hydrogels were characterized for physical and biological properties. Based on the antibacterial determination, the 1 and 5 mM nAg–embedded PVP hydrogels were effective, with 99.99% bactericidal activity at 12 h and 6 h, respectively. The indirect cytotoxicity evaluation based on MTT assay indicated that both the neat and the nAg–embedded PVP hydrogels were non-toxic to mouse fibroblasts (L929). The 5 mM nAg-embedded PVP hydrogels not only provided a clean, moist environment for wound healing but also effectively prevented bacterial infection and enhanced wound recovery.

Keywords: hydrogels; silver nanoparticles; poly(vinyl pyrrolidone); gamma irradiation; wound dressing

3.2 Introduction

Wounds can be classified according what caused the wound: abrasions, incisions, lacerations, punctures, or burns. Once a skin lesion occurs, the normal process of healing is instantly set in motion to compensate for that damage. The wound healing process is commonly divided into three or four overlapping phases: hemostasis, inflammation, proliferation, and remodeling [1-4]. During these complex biochemical events, infections happen at a high rate of incidence. Larger breaks in the skin have a higher risk of developing an infection. However, infections can also occur in small wounds, from poor hygiene or in people with impaired immune defense systems. Normal bacteria that are localized on the skin (normal flora) often enter a wound first. Breaks in the skin allow bacteria a chance to enter the skin and multiply, invade, damage the surrounding tissue, and cause infection. Bacteria may also come from the surrounding environment. More than one type of bacteria may infect the same wound simultaneously. These infections can cause by *Staphylococcus aureus* (*S. aureus*) and *Streptococcus pyogenes* (*S. pyogenes*). Others organisms; *Streptococcus epidermidis* (*S. epidermidis*), *Streptococcus agalactiae* (*S. agalactiae*), *Escherichia coli* (*E. coli*), and *Pseudomonas aeruginosa* (*P. aeruginosa*) are occasionally involved [5]. An infected wound will lengthen the healing process, specifically by stimulating an inflammatory response [6]. Therefore, proper healing without infection should be a priority.

Among the numerous metal nanoparticles well recognized as effective antibacterial agents in biomedical applications, silver nanoparticles (nAg) exhibit broad antibacterial activity. Bactericidal effects can be achieved by a proposed mechanism; release of charged silver atoms (ionic silver) in contact with wound fluid are preferentially bound to microbial DNA causing DNA denaturation and replication inhibition [7]. Furthermore, adenosine triphosphate (ATP) synthesis can be inhibited due to the binding of silver ions with ATP synthase [7-11]. In addition to its superior antimicrobial properties, silver also has the added benefit of regulating the local matrix metalloproteinase (MMP) to optimum levels that can facilitate healing. Matrix metalloproteinase is a group of collagenase enzymes that are required in the healing process, but excess levels can degrade the fibronectin and

peptide growth factor [12]. Hence, silver-based wound dressings are particularly effective for maintaining a microbe-free environment and aiding wound treatment [13]. However, the release of toxic biocides is a concern when using silver nanoparticles [14, 15]. Because of this restriction, it is necessary to find a method to develop a silver-containing dressing that is non-toxic and environmental friendly.

With ongoing research, various approaches have been taken for nAg synthesis: chemical reduction, microorganism reduction, microwave-assisted, photochemical reduction, and laser ablation [8-10, 14, 16-24]. Apart from the above-mentioned methods, the use of a gamma-irradiation technique has been extensively studied. Gamma rays are high energy photon, which commonly used for sterilization due to the high penetration power. Hence, the operation must be operated and protected strictly. The gamma-irradiation process has several advantages, such as uncomplicated process control and environmental friendliness (since it leaves no waste or residual byproducts and has no required initiators or cross-linking agents that are detrimental or difficult to remove). These advantages also allow for a process that does not require any further purification [25]. Especially, hydrogel formation, metal ion reduction and sterilization can occur in one processing step allowing the gamma-irradiation technique to become a desirable technique for incorporating nAg into hydrogel wound dressings.

Poly(vinyl pyrrolidone) (PVP) is a biodegradable polymer that is commonly used in biomedical applications. Moreover, it is recognized as one of the most outstanding polymeric stabilizing agents for nAg [16, 17, 26-29]. In this work, nAg-embedded PVP hydrogels were prepared as antibacterial wound dressings with the gamma-irradiation technique. The physical properties, release characteristics, antibacterial properties, indirect method of cytotoxicity, and *in vivo* wound healing tests of nAg-embedded PVP hydrogels were assessed.

3.3 Materials and Methods

3.3.1 Chemicals

Poly(vinyl pyrrolidone; Mw 1,360,000 Da) was obtained from Aldrich. Silver nitrate ($AgNO_3$; 99.998% purity) was bought from Fisher Scientific

(USA). Polyethylene glycol (PEG; Mw 6,000) was purchased from Univar. Isopropyl alcohol (IPA; 99.8% purity) was purchased from Merck. All chemicals were used without additional purification.

3.3.2 Microorganisms

Gram-negative bacteria: *Acinetobacter iwoffii* (*A. iwoffii*, ATCC 15309), *Escherichia coli* (*E. coli*, ATCC 25922), *Pseudomonas aeruginosa* (*P. aeruginosa*, ATCC 27853) and gram-positive bacteria: *Bacillus cereus* (*B. cereus*, ATCC 11778), *Staphylococcus aureus* (*S. aureus*, ATCC 25923), *Staphylococcus aureus* (MRSA, DMST 20654), *Staphylococcus epidermidis* (*S. epidermidis*, ATCC 12228), and *Streptococcus pyogenes* (*S. pyogenes*, DMST 17020) were used for the experiment.

3.3.3 Cell Culture

Mouse fibroblastic cells (L929) were used as reference cells. The formulation of the culture media contained Dulbecco's modified Eagle's medium (DMEM) with 10 % fetal bovine serum (FBS), 1 % L-glutamine, and 1 % antibiotic, and an antimycotic formulation (combination of penicillin G sodium, streptomycin sulfate, and amphotericin B) were purchased from Invitrogen Corp., USA. Ethanol was purchased from Labscan (Ireland).

3.3.4 Preparation of Neat and nAg-embedded PVP Hydrogel Pads by γ-irradiation

A base PVP solution was prepared at a concentration of 12% (w/v) by dissolving PVP powder in distilled water at 45 °C under mechanical stirring until the PVP solution became clear. Subsequently, $AgNO_3$ powder was added to the base PVP solution to obtain the final Ag concentrations of 1, 5, 10, 50, and 100 mM. Polyethylene glycol (PEG; 2 %w/v) and 0.5 M IPA were then added to the solution as a plasticizer and hydroxyl radical scavenger, respectively. Prior to gamma irradiation, the solutions were sealed in nylon bags. All experiments were assessed at ambient temperature (25 °C). These solutions were then exposed to gamma irradiation from a cobalt-60 source at 25, 35, and 45 kGy to allow the formation of Ag nanoparticles and crosslinking of PVP hydrogels simultaneously. For the neat PVP hydrogel pads, $AgNO_3$ powder was not added to the base PVP solution.

3.3.5 Characterization and Testing

3.3.5.1 Formation, Size, and Distribution of nAg

The formation of nAg in the PVP hydrogels, after being exposed to γ-irradiation, was confirmed by the presence of the surface plasmon resonance at a wavelength of ~400 nm, by a UV-VIS spectrophotometer; model UV-1800. The shape, size, and distribution of the nAg were investigated with a transmission electron microscope (TEM) model JEM-2100, JEOL, and scanning electron microscopy (SEM); model HITACHI S-4800, with energy-dispersive X-ray (EDX); model HORIBA EMAX X-actodetector.

3.3.5.2 Gel Fraction

The gel fractions of the neat and nAg-embedded PVP hydrogels were evaluated by measuring their insoluble part after extraction from hot distilled water. The dried hydrogel specimens were totally immersed in 60 °C distilled water for ~24 h, extracted, and dried at 60 °C for another ~24 h until their weight was constant. The gel fraction was calculated according to the equation:

$$\text{Gel fraction (\%)} = \left(\frac{W_d}{W_i}\right) \times 100 \quad (1)$$

where W_i is the dry gel weight before and W_d is the dry gel weight after extraction.

3.3.5.3 Water Absorption and Weight Loss Behavior

Water absorption and weight loss behavior of the neat and nAg-embedded PVP hydrogels were carried out by total submersion in buffer solution; simulated body fluid (SBF; pH 7.4) at a human body temperature of 37 °C. After the equilibrium swelled, water absorption and weight loss were also calculated by the following equations:

$$\text{Water absorption (\%)} = \left(\frac{W_s - W_i}{W_i}\right) \times 100 \quad (2)$$

$$\text{Weight loss (\%)} = \left(\frac{W_i - W_d}{W_i}\right) \times 100 \quad (3)$$

where W_s is the weight of each swollen sample after submersion in SBF at each time interval, W_i is the initial dry weight of the sample and W_d is the dry weight of the sample after submersion in SBF solution at each time interval.

3.3.5.4 Water Vapor Transmission Rate

The water vapor transmission rate (WVTR) was measured based on the European Pharmacopoeia Standard. The neat and nAg-embedded PVP hydrogel samples (diameter 40 mm) were sealed as a cap of glass container filled with 25 ml distilled water. The container was then kept in an oven at a constant temperature of 35 °C for 24 h. The WVTR was calculated by using the equation:

$$\text{WVTR} = \left(\frac{W_i - W_t}{A \times 24}\right) \times 10^6 \quad (4)$$

where A is the container mouth area (mm^2), W_i is the weight of container before being placed in the oven, and W_t is the weight of the container after being placed in the oven.

3.3.5.5 nAg Release Assay

The actual content of silver (either Ag^+ ions or nAg) in the nAg-embedded PVP hydrogels (15 mm diameter) was investigated. First, the specimens were immersed in a 5 ml solution of 95% nitric acid (HNO_3), and a SBF (pH 7.4) solution was added to achieve a final volume of 50 ml. It was kept under vigorous stirring and shaking in an incubator for 24 h. Then, the amount of silver in the obtained solution was measured by a Varian SpectrAA-300 atomic absorption spectroscope (AAS).

For the release assay, the dried sample discs of nAg-embedded PVP hydrogels were totally submerged in 20 ml of simulated body fluid (SBF) at 37 °C. SBF was used as a releasing medium to simulate human body fluid (pH = 7.4) (procedure for preparing SBF is available as Supplementary data). At each submersion time point, between 0 h and 360 h, the buffer solution was removed and an equal amount of fresh buffer was replaced to keep the system volume constant. The amounts of released silver in the withdrawn buffer solution were also measured by AAS. The measurements were performed in triplicate. The results were

calculated to the cumulative amounts of the released silver, based on the unit weight of the hydrogel specimens.

3.3.5.6 Antibacterial Determination

3.3.5.6.1 The Disc Diffusion Method

Antibacterial activity of the neat and nAg-embedded PVP hydrogels was evaluated against common skin pathogens according to the disc diffusion method of the US Clinical and Laboratory Standard Institute (CLSI). The bacteria in this study were gram-negative bacteria: *A. iwoffii*, *E. coli*, and *P. aeruginosa*, and gram-positive bacteria: *B. cereus*, *S. aureus*, MRSA, *S. epidermidis*, and *S. pyogenes*. The neat PVP hydrogel was used as a control. The 18 h microbial culture in Difco™ Muller-Hinton broth was diluted to approximately 10^5 CFU/ml with 0.85% (w/v) normal saline solution. The microbial solutions were spread over the Difco™ Muller-Hinton agar plates. Each specimen (15 mm diameter) was placed on microorganism-cultured agar plates and incubated at 37 °C for 24 h. The zone of inhibition was monitored.

3.3.5.6.2 The Dynamic Shake Method

The quantitative antibacterial evaluation of the neat and nAg-embedded PVP hydrogels was carried out based on the viable microorganisms from the treatment of the antimicrobial specimens under a dynamic contact condition. This antibacterial activity was evaluated against *Staphylococcus aureus* (*S. aureus*)—gram-positive bacteria are generally found in contaminated wounds—with inoculum prepared by suspending one colony of *S. aureus* in 20 ml of nutrient broth. Then, the broth was placed in a shaker-incubator at 37 °C for 24 h. One milliliter of the suspension was withdrawn and made into a serial dilution with sterilized saline solution. Each specimen of the neat and nAg-embedded PVP hydrogels was immersed in 10^7 CFU/ml of diluted inoculum with constant agitation at 0 h, 3 h, 6 h, 12 h, and 24 h contact times. After each contact time, 100 µl of these suspensions was withdrawn and arranged in a spiral on sterilized nutrient agar in a petri dish (in triplicate). Bacterial growth was observed after overnight incubation at 37 °C in a shaker-incubator. The number of viable bacteria was determined and the bacterial reduction rate at specific contact times was calculated according to the following equation:

$$\text{Bacterial reduction rate (\%)} = \left(\frac{B-A}{B}\right) \times 100 \quad (5)$$

where A is number of colonies in the test group (nAg-embedded PVP hydrogels) and B is number of colonies in the control group (neat PVP hydrogels).

3.3.5.7 Indirect Cytotoxicity Assay

The indirect cytotoxicity evaluation of the neat and nAg-embedded PVP hydrogels was carried out by an adaptation of the ISO10993-5 standard test method, using mouse fibroblastic cells (L929) as reference cells. The L929 cells were first cultured in DMEM. The culture medium was removed and replaced every 3 days and the cultures were incubated at 37 °C in a humidified atmosphere containing 5% CO_2.

The nAg-embedded PVP hydrogels weighed ~0.02 g each. Before the experiment, each sample was sterilized with 70% (v/v) ethanol for 30 min. To remove the ethanol, the samples were washed with autoclaved deionized water, then phosphate buffer saline (PBS). Subsequently, extraction media were produced by immersing each sample in serum-free medium (SFM; which contained DMEM) at the extraction ratio of 10 mg/ml in each well of the cell culture plates for one, two, and three days. The cultured mouse fibroblastic cells were trypsinized (0.25% trypsin with 1 mM EDTA), counted with a hemocytometer, and seeded in the serum-containing DMEM with a density of ~10,000 cells per well. Cells were allowed to adhere and spread over the well bottoms after incubation at 37 °C for ~16 h. The attached cells were serum-starved for another 24 h. Finally, cells were cultured with an as-prepared extraction media (test group) and with fresh SFM (control group) prior to the investigation of the viability of the cells by using 3-(4,5-dimethylthiazol-2-yl)-2,5-diphenyltetrazolium bromide (MTT) assay.

The principal of MTT assay is that tetrazolium salt (yellow color) is oxidized to formazan crystals (purple color) by mitochondrial dehydrogenase enzymes of living cells. The quantity of the produced formazan crystals and living cells are in direct proportion. Briefly, after the incubation of cells culture, either extraction media or fresh SFM was removed before adding 300 µl/well

of MTT solution at 0.5 mg/ml for a cell culture plate 96 well. Subsequently, the plate was incubated at 37 °C for 10 min to 30 min to obtain violet crystals at the bottom. The solution was then replaced with 1 ml dimethyl sulfoxide (DMSO)/glycine buffer in each well and the plate was agitated for 10 min in order to dissolve the formazan crystals. Finally, absorption was detected by a SpectraMax M2 microplate reader at a wavelength of 570 nm, demonstrating the cell viability.

3.3.5.8 Wound Healing Assessment

The in vivo wound healing test was approved by the Ethics Committee of the Faculty of Veterinary, Chulalongkorn University (No. 12310042). The animal experiments were performed according to the Institutional Animal Care and Use Committee (IACUC) under standard sterile conditions. An *in vivo* wound healing evaluation was carried out with 15 male Wistar rats (10 weeks of age). All experimental rats were distributed into three groups, corresponding to the following experimental treatments: Group A as a control, Group B with neat PVP hydrogel, and Group C with 5 mM nAg-embedded hydrogels. A full-thickness skin wound of 1 cm diameter was made on the dorsum of the body of each rat. The rats were randomly divided into three groups. For Group A, only non-adherent dressings were applied to the wound (Melolin®) and occlusive dressings (Hypafix®) were utilized as a control. In Group B and Group C, neat PVP hydrogels and 5 mM nAg-embedded hydrogels were applied, respectively, and then covered with Melolin® and Hypafix®. Dressings were replaced every two days during the 12-d study (n=5 per experimental group per dressing change). The percentages of wound area and macroscopic examination were investigated on days 0, 2, 4, 6, 8, 10, and 12.

3.4 Statistical Analysis

All data are in the form of means ± standard errors of means (n = 3). Statistical analysis was achieved by SPSS 17.0 using ANOVA and followed by Scheffe's post hoc test. The acceptable statistical significance was a 0.05 confidence level.

3.5 Results and Discussion

3.5.1 Formation, Size, and Distribution of Silver Nanoparticles

The presence of absorption spectra at ~400 nm, according to the surface plasmon resonance effect, is indicated for the occurrence of spherical nAg [30]. Figure 3.1 shows the representative absorption spectra of the as-formed nAg on gamma irradiation of $AgNO_3$-PVP aqueous solution at 35 kGy. Thus, the characteristic peaks of nAg at 402-413 nm were clearly observed for both 1 and 5 mM nAg-embedded PVP hydrogels after having been exposed to gamma irradiation at various doses. Consequently, such a peak was not present in the neat PVP hydrogels. Moreover, the intensity of the UV absorption peak was increased, indicating a larger amount of nAg with increasing $AgNO_3$ concentrations in PVP aqueous solution [31, 32].

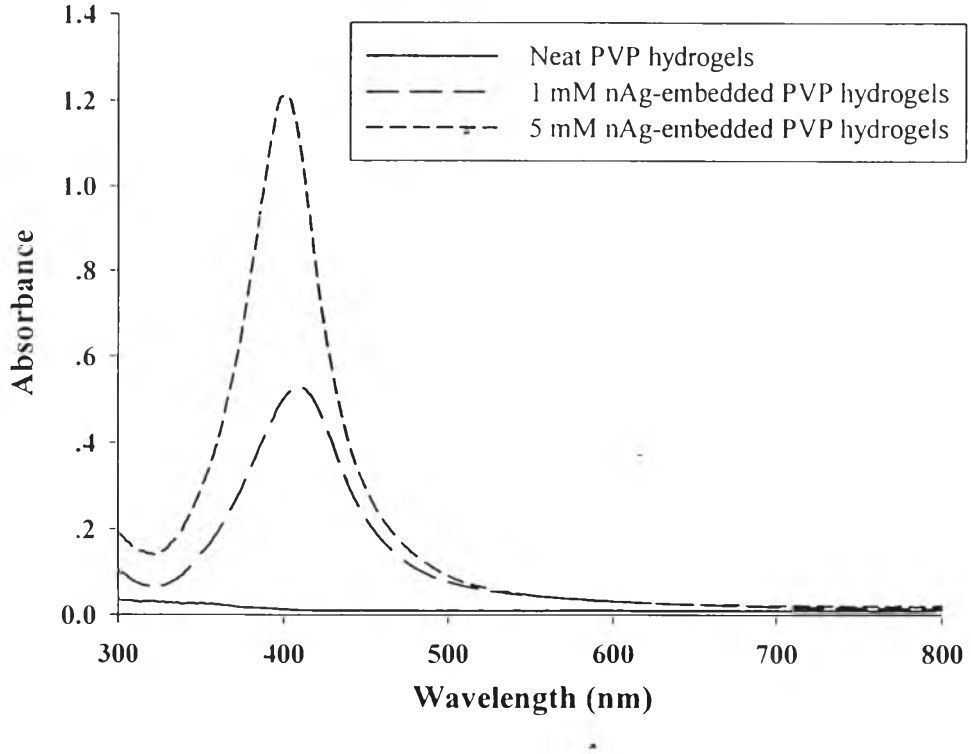

Figure 3.1 Representative UV-visible absorption spectra of nAg-embedded PVP hydrogels at various $AgNO_3$ concentrations, irradiated at 35 kGy.

Furthermore, TEM and SEM-EDX were used to confirm that nAg was well distributed and had a spherical shape in the 4-10 nm range (Figure 3.2). In addition, Figure 3.2b shows i) electron image of hydrogels ii) distribution of carbon, iii) distribution of oxygen, and iv) distribution of nAg in 5 mM nAg-embedded PVP hydrogels after having been irradiated at 25 kGy.

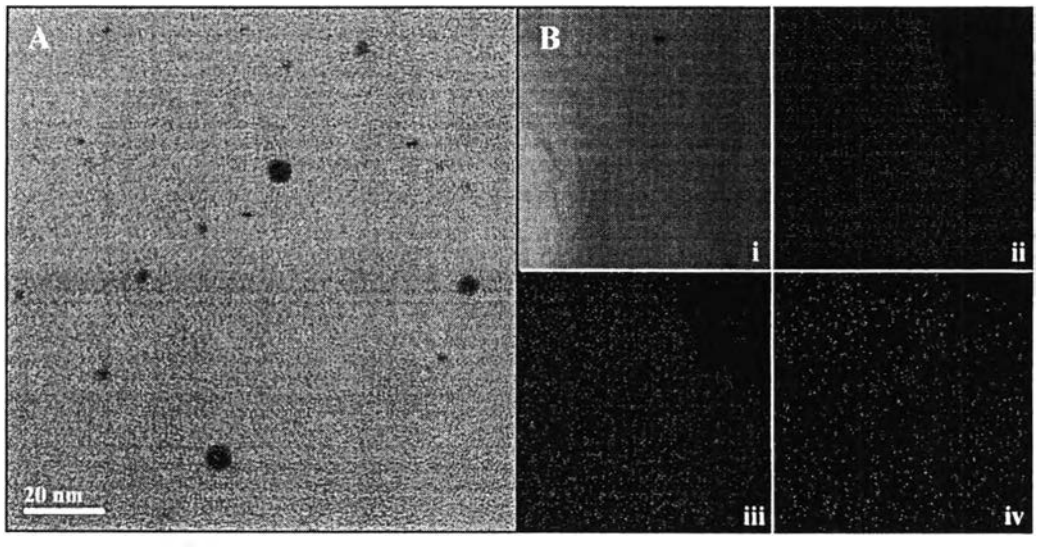

Figure 3.2 Representative (a) TEM micrograph of 5 mM nAg-embedded PVP hydrogels and (b) SEM-EDX images of i) electron image of hydrogels ii) distribution of carbon, iii) distribution of oxygen, and iv) distribution of nAg in 5 mM nAg-embedded PVP hydrogels after having been irradiated at 25 kGy.

3.5.2 Gel Fraction

Various concentrations of $AgNO_3$-embedded PVP aqueous solutions were exposed to doses of gamma irradiation—25, 35 and 45 kGy. Generally, gamma irradiation of 25 kGy is the minimum dose applied to ensure sterility of a sample [33]. Interestingly, at the given radiation doses, the 10 mM, 50 mM, and 100 mM, the $AgNO_3$- PVP aqueous solutions could not be transformed into hydrogel. This could be described by the following radiolytic reduction mechanisms: nAg formation and cross-linking of PVP. When aqueous solutions are irradiated with gamma ray, large amounts of hydrated electrons (e^-_{aq}) and $H^{\cdot}$ atoms are generated [34]:

$$H_2O \xrightarrow{\gamma-rays} e^-_{aq}, H_3O^+, H^{\cdot}, H_2, OH^{\cdot}, H_2O_2 \qquad (6)$$

Then, the hydrated electrons (e^-_{aq}) reduces Ag^+ ions to neutral Ag^0 atoms (equation 7) and The neutral atom Ag^0 is found to react with Ag^+ ions to form relatively stable Ag clusters [35, 36] (equation 8-10):

$$Ag^+ + e^-_{aq} \xrightarrow{\text{reduction}} Ag^0 + H_2O \quad (7)$$

$$Ag^0 + Ag^+ \rightarrow Ag_2^+ \quad (8)$$

$$nAg^+ + Ag_2^+ \rightarrow (Ag)_n^+ \quad (9)$$

$$(Ag)_n^+ + ne^-_{aq} \rightarrow (Ag)_n \quad (10)$$

Concurrently, cross-linking of PVP can also occur when the generated radicals react with PVP chain resulting in the PVP hydrogel network. According to radiation mechanism of nAg formation and PVP crosslinking, it can be implied that the PVP aqueous solutions with a high $AgNO_3$ concentration required a gamma irradiation dose higher enough to achieve both nAg formation and hydrogel formation simultaneously [37]. For 0, 1, and 5 mM nAg-embedded PVP hydrogels after irradiation, the typical dependences of gel fraction are given in Figure 3.3. The results show that the gel fraction was slightly increased with increasing irradiation doses due to the higher crosslinking degree of the polymer network at high irradiation doses of 25 to 45 kGy. In contrast, the gel fraction decreased with increasing $AgNO_3$ concentration. The more the $AgNO_3$ concentrations were embedded; the more energy was required to reduce the Ag^+ ions to Ag^0. Consequently, the energy that remained was used to crosslink the hydrogel network. Hence, increasing the $AgNO_3$ concentration in the PVP solution resulted in a decrease of hydrogel gel fractions.

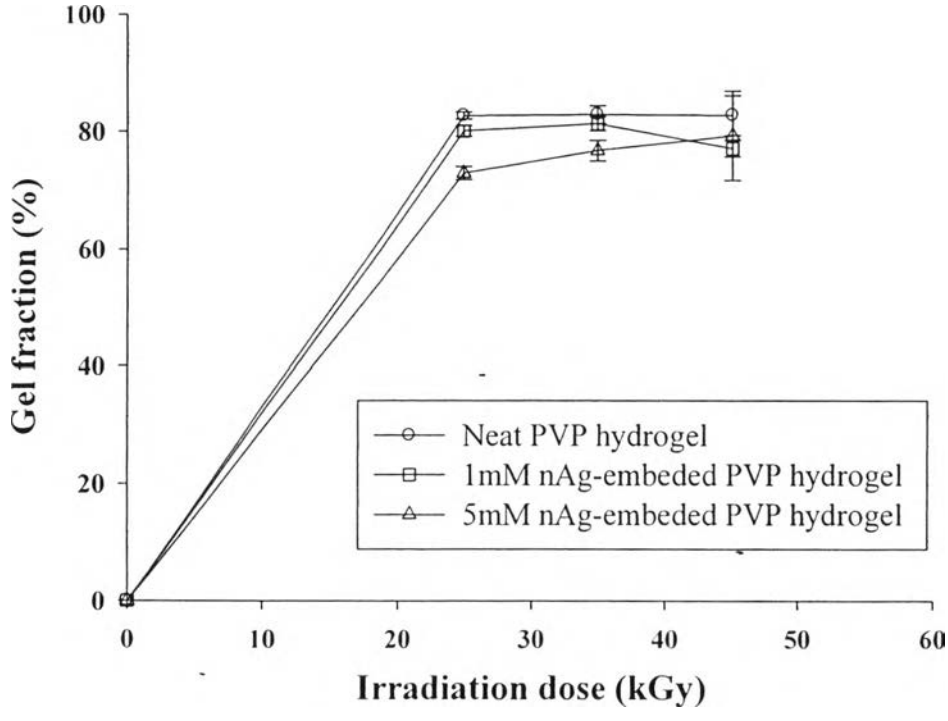

Figure 3.3 Gel fraction of neat and nAg-embedded PVP hydrogels at various irradiation doses.

3.5.3 Water Absorption and Weight Loss Behaviors

With exposure to a high humidity environment by the hydrogel wound dressing, water absorption and weight loss behaviors were investigated. Rattanaruengsrikul *et al.*[10] reported that the retention of water in the nAg-loaded gelatin hydrogel pads in SBF buffer was a maximum of ~997% and the weight loss of hydrogels ranged from 9 % to 49 %. When comparing the nAg-embedded PVP hydrogels, as shown in Figure 3.4, the water absorption ranges are between 2200 and 3200% and the weight loss of hydrogels average ~18%. The water absorption and % weight loss decreased with an increase in the gamma irradiation dose applied to the $AgNO_3$-PVP aqueous solution, leading to a greater gel fraction of the nAg-embedded PVP hydrogels [38, 39]. In contrast with increasing $AgNO_3$ concentration in the PVP aqueous solution, both behaviors increased due to the lower gel fraction in polymer network.

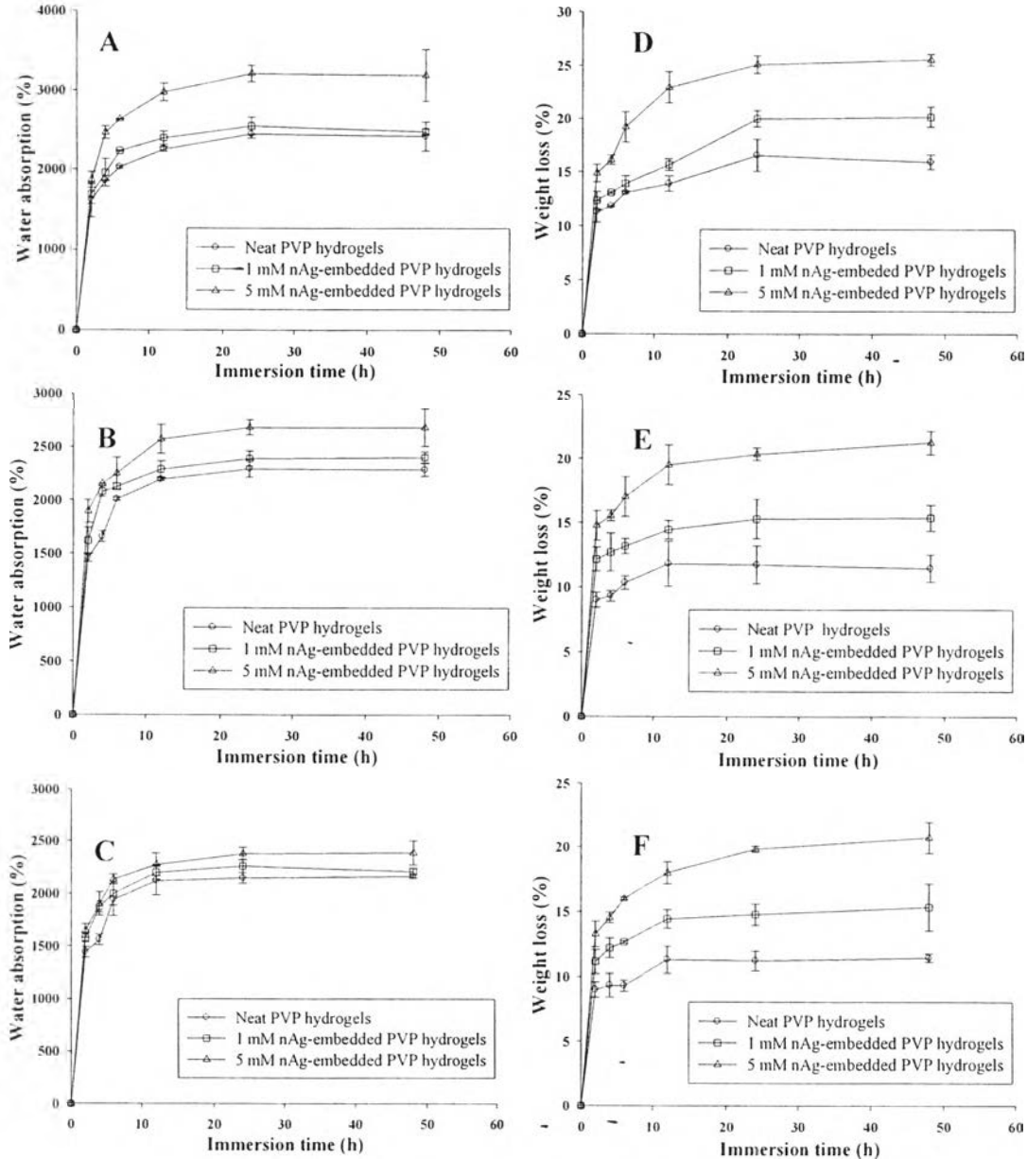

Figure 3.4 Water absorption (%) of nAg-embedded PVP hydrogels at various $AgNO_3$ concentrations after been irradiated at (a) 25, (b) 35 and (c) 45 kGy. Weight loss behaviors of nAg-embedded PVP hydrogels at various $AgNO_3$ concentrations after been irradiated at (d) 25, (e) 35 and (f) 45 kGy.

3.5.4 Water Vapor Transmission Rate (WVTR)

The key characteristic of ideal wound dressings is optimum WVTR, the removal of excess wound exudate while providing optimum moisture at the

wound site [40]. Lamke, et al. (1977) stated that water evaporation loss ($g/m^2/day$) of normal skin is 204 and this value can increase in damaged skin from 279 (first degree burn) up to 5138 (granulating wound). Due to the varying water evaporation loss for each type of wound, there are no universal dressing materials that can be applied for all wound types. The WVTR compared to water evaporation loss of a wound is the value that should not be too high or it will cause wound dehydration. Conversely, the WVTR value should not be too low, or exudates will accumulate and cause bacterial infection which can retard the wound healing process. In this work, the WVTR of the 3.5 mm thick nAg-embedded PVP hydrogels was in the range of 643 $g/m^2/d$ to 940 $g/m^2/d$ as shown in Table 3.1. The WVTR value ($g/m^2/d$) in this study is comparable to that of Duoderm (886) and Metoderm (823) [41]. The irradiation dose and $AgNO_3$ content had no significantly effect on the WVTR values. Therefore, the nAg-embedded PVP hydrogels that had been irradiated at 25kGy were suitable for skin wound dressings due to the favorable gel properties (%gel fraction, %water absorption, %weight loss and water vapor transmission rate). Moreover, in terms of energy consumption, the $AgNO_3$-PVP aqueous solution gamma irradiated with 25 kGy required less energy compared to 35 and 45 kGy nAg-embedded PVP hydrogels.

Table 3.1 Water vapor transmission rate (WVTR) of neat and nAg-embedded PVP hydrogels at various irradiation doses

Sample	WVTR ($g/m^2/d$)		
	25 kGy	35 kGy	45 kGy
Neat PVP hydrogel	733.53	727.78	642.93
1 mM nAg-embedded PVP hydrogel	783.52	716.58	714.54
5 mM nAg-embedded PVP hydrogel	940.16	787.26	764.50

3.5.5 Silver Nanoparticles Release Assay

The theoretical content of silver within nAg-embedded PVP hydrogels, which had been produced from PVP solution containing 1 and 5 mM of

$AgNO_3$, were about 0.1079 mg/g and 0.5395 mg/g, respectively. If these amounts were the total amount of silver released from the hydrogels, the concentration of silver in the medium would have been 5.4 ppm/g (1 mM) and 17.9487 ppm/g (5mM) of sample, respectively. The cumulative amount of Ag, either Ag nanoparticles or residual free ion form that were released from the nAg-embedded PVP hydrogels was reported by the amount of released Ag ions (in ppm) divided by the weight of the specimens (g) as a function of submersion time (Figure 3.5). The cumulative released amounts of silver from 1 and 5 mM nAg-embedded PVP hydrogels were about 1.2 ppm/g and 15 ppm/g of hydrogels, respectively, according to a concentration gradient in the system. In addition, the first period of submersion showed rapid release and a subsequently slower release for both hydrogel samples. The nAg-embedded PVP hydrogels that had been irradiated with 25 kGy showed the highest cumulative released amount because there was a lower degree of cross-linking; therefore, it was chosen for further investigation.

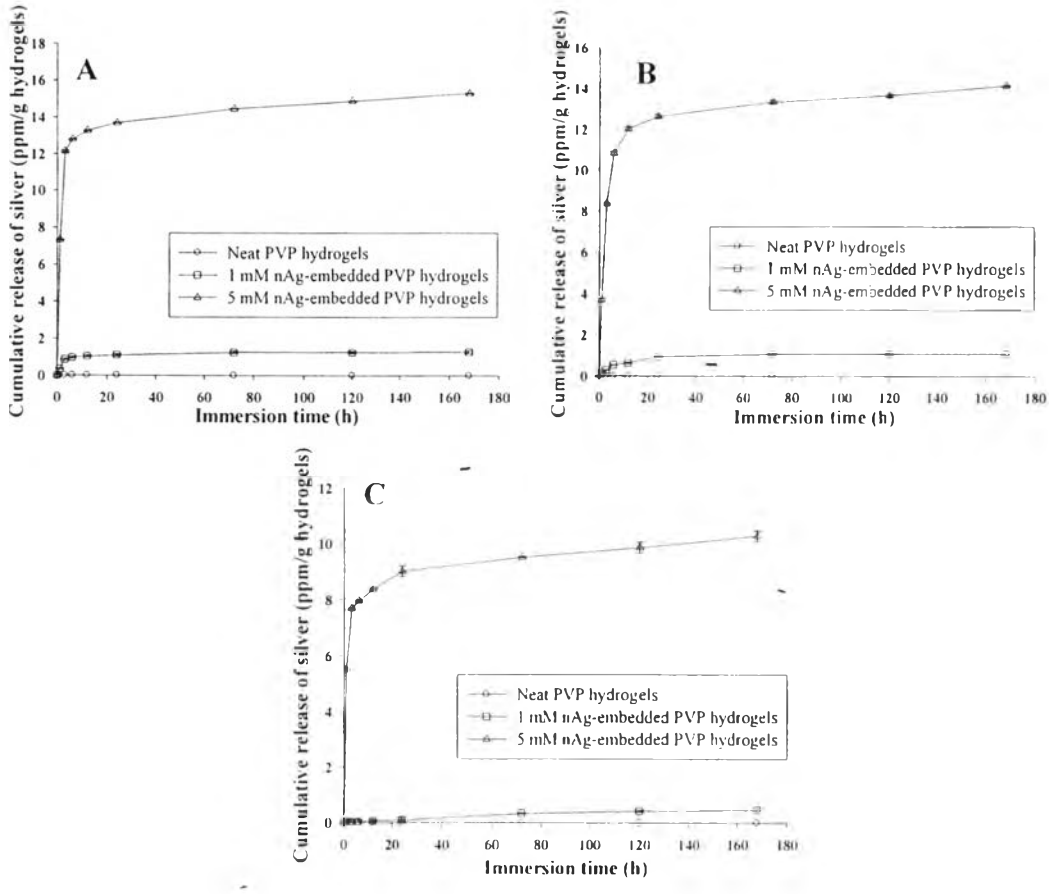

Figure 3.5 Cumulative release profile of silver from 1 mM and 5 mM nAg-embedded PVP hydrogels after having been irradiated at dose (a) 25, (b) 35 and (c) 45 kGy (reported as the amount of the released silver divided by the actual weight of the specimens (ppm/g) in phosphate buffer saline solution (PBS) at the physiological temperature of 37 °C (n=3)).

3.5.6 Antibacterial Determination

3.5.6.1 The Disc Diffusion Method

The antibacterial activity of neat and nAg-embedded PVP hydrogels was assessed against gram-negative bacteria: *A. iwoffii*, *E. coli*, *P. aeruginosa*, and gram-positive bacteria: *B. cereus*, *S. aureus*, MRSA, *S. epidermidis*, and *S. pyogenes*. In a previous work, Rujitanaroj *et al.*[9] reported that the nAg-containing electrospun gelatin fiber mats had antibacterial activity against *S. aureus*, MRSA, *P. aeroginosa*, and *E. coli*. [9]. In this work, the neat PVP hydrogels was

used as a control; no inhibition zone was observed. The 5 mM nAg-embedded PVP hydrogels exhibited inhibition zones against all tested bacteria; *B. cereus*, *S. aureus*, MRSA, *S. epidermidis*, *S. pyogenes, A. iwoffii*, *E. coli*, and *P. aeruginosa*,. The 1 mM nAg-embedded PVP hydrogels showed smaller inhibition zones for only three strains: *A. iwoffii, S. epidermidis*, and *S. pyogenes*. The diffusion of Ag ions by the nAg-embedded PVP hydrogels on the bacterial agar plate may have been affected by many factors: nAg content, irradiation dosage, and physical properties of both the Ag nanoparticles and hydrogels. Therefore, the dynamic shake method should be completed for quantitative analysis of antibacterial activity.

3.5.6.2 The Dynamic Shake Test Method

Figure 3.6 shows the nAg-embedded PVP hydrogels, after having been irradiated at 25 kGy, and the effects of Ag nanoparticle content and contact time on the bactericidal efficacy of 1 and 5 mM nAg-embedded PVP hydrogels against *Staphylococcus aureus*. The results show that the bacterial reduction rate increased with increasing nAg content and contact time. Correspondingly, the contact times of 12 h and 6 h were satisfactory to obtain 99% reduction in the 1 mM and 5 mM nAg-embedded PVP hydrogels, respectively. Whereas Wu *et al.* obtained the 100% reduction in viable *S. aureus* on the AgNP-BC hybrid gel-membranes after 24 h of incubation [23].

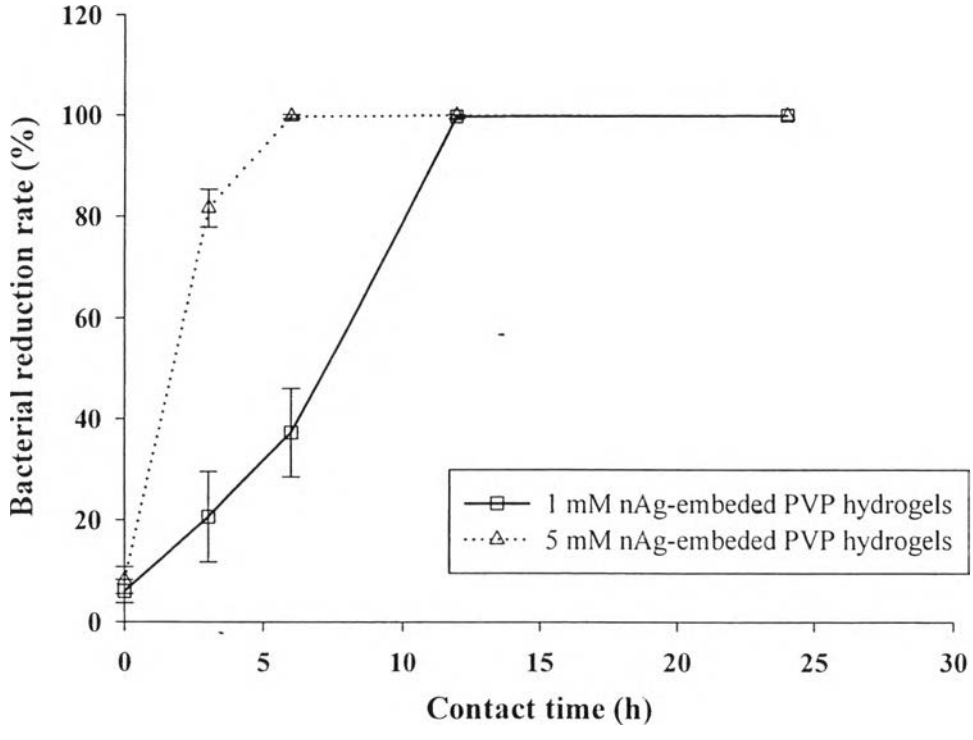

Figure 3.6 Bacterial reduction rate (%) of *Staphylococcus aureus* after incubation with nAg-embedded PVP hydrogels.

3.5.7 Indirect Cytotoxicity Assay

The effectiveness of the nAg-embedded PVP hydrogels as a wound dressing was investigated for cytotoxicity of this material, using mouse fibroblastic cells (L929) as reference cells. As can be seen in Figure 3.7, the cells cultured with the extraction media, which was prepared from either neat or nAg-embedded PVP hydrogels, after having been irradiated at 25 kGy, exhibit cell viability of greater than 80% as compared to those with the fresh SFM media. It can be concluded from the result that these materials are non-toxic toward L929 cells.

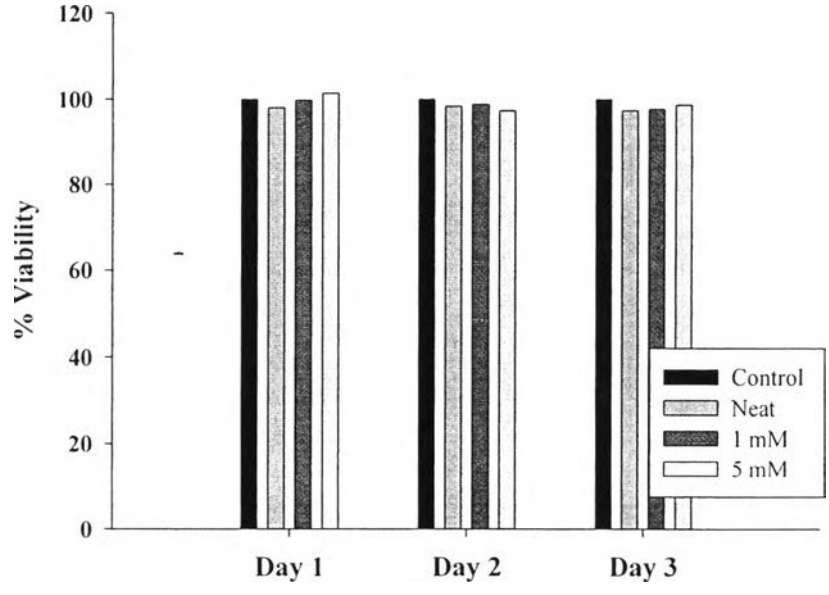

Figure 3.7 Viabilities of mouse fibroblastic cells (L929) that were cultured for 1, 2, and 3 days with extraction media concentration of 10 mg/ml from neat and nAg-embedded PVP hydrogels (25 kGy) in comparison with viability of the cells that were cultured with fresh culture medium (n = 3).

3.5.8 Wound Healing Assessment

Figure 3.8 shows the percentage of wound area compared with the original wound size, which shown in Figure 3.9. It was discovered that on days 2 to 4, the percentages of wound area of Group B and Group C were lower than Group A. This is plausibly because both the optimized moisture in the wound area of the hydrogel and the antibacterial activity of the nAg can promote wound healing. Between days 6 to 12, within the proliferative phase, all experimental groups had comparable decreases in wound size. This can imply that wound contraction also occurs during the proliferative phase, leading to a smaller wound size. Moreover, the antibacterial activity was not present in any significant amounts, since wound infection normally occurs during the inflammatory phase.

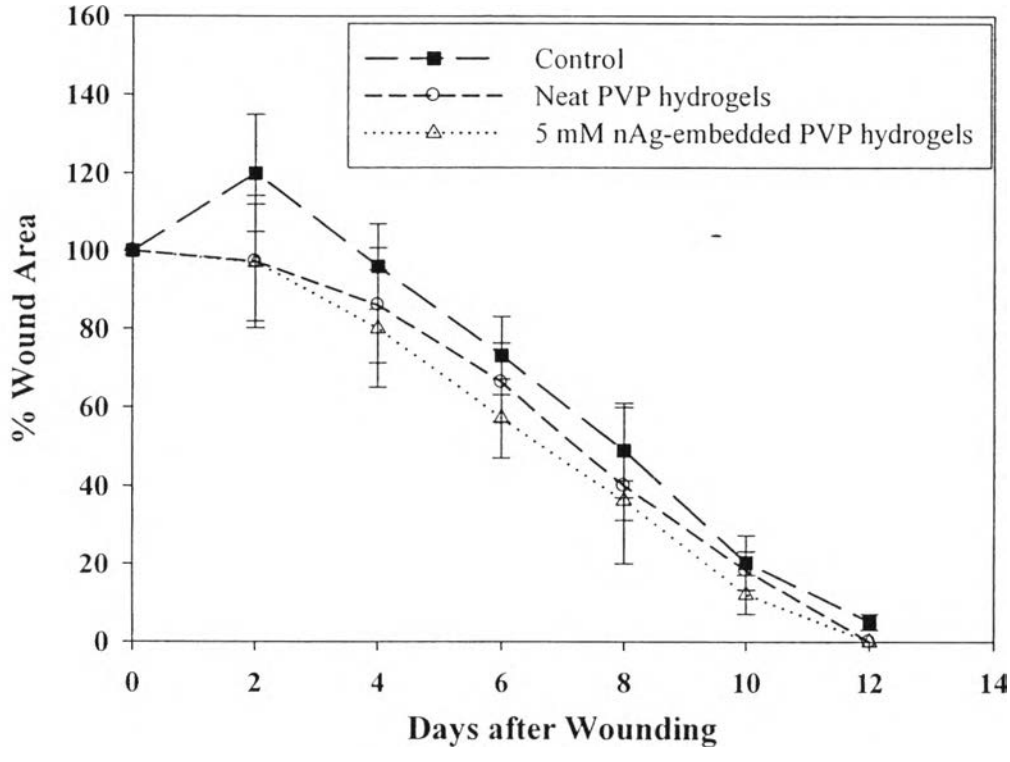

Figure 3.8 Time course of wound closure in rats: Group A was applied with conventional wound dressing, Group B with neat PVP hydrogels, and Group C with 5 mM nAg-embedded PVP hydrogels.

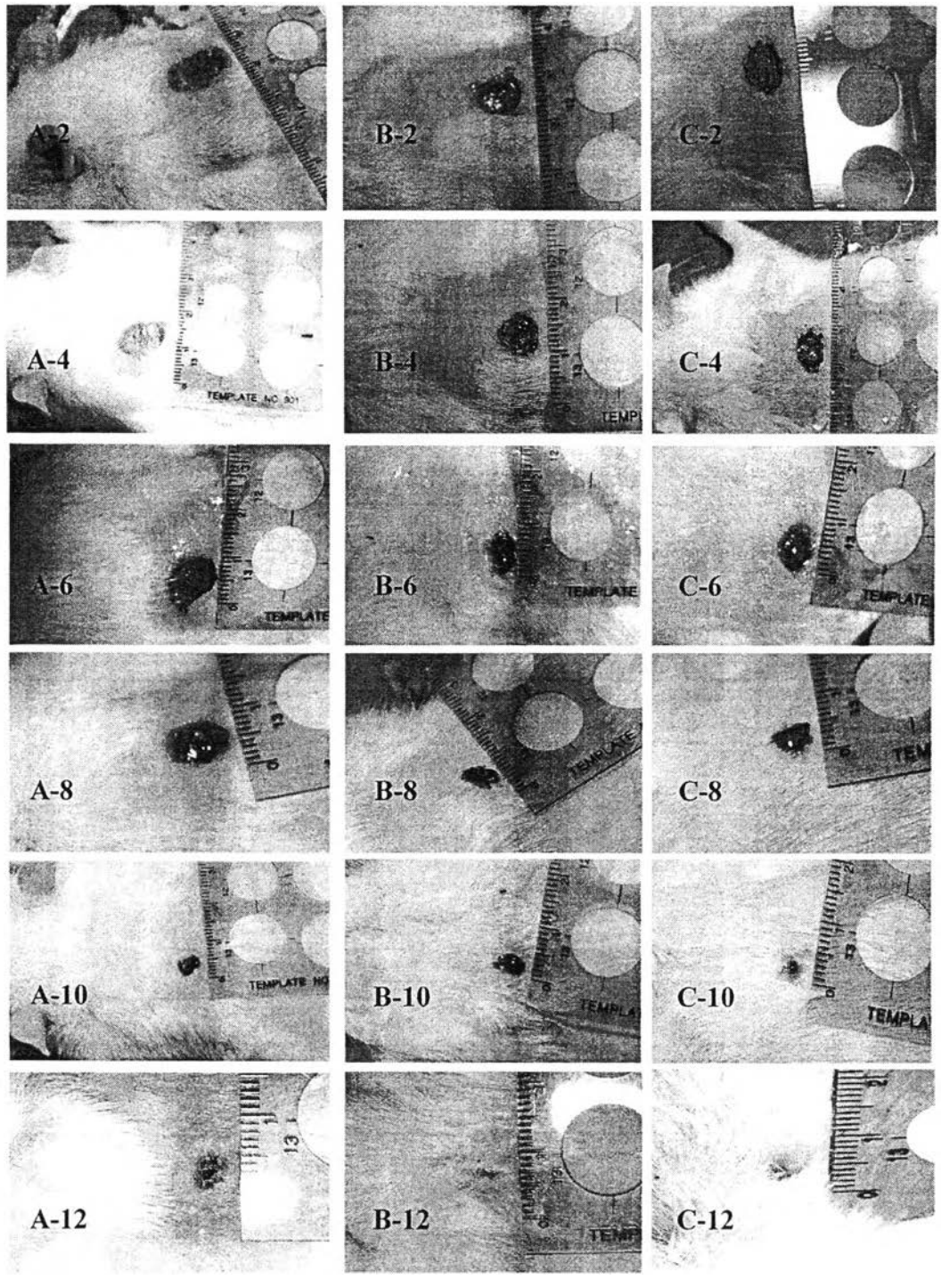

Figure 3.9 Macroscopic examinations of wound healing at various times during the healing process: Group A at day 2, 4, 6, 8, 10 and 12 (A-2, A-4, A-6, A-8, A-10, and A-12), respectively, Group B at day 2, 4, 6, 8, 10 and 12 (B-2, B-4, B-6, B-8, B-10, and B-12), respectively, and Group C at day 2, 4, 6, 8, 10 and 12 (C-2, C-4, C-6, C-8, C-10, and C-12), respectively.

3.6 Conclusions

The neat, 1 mM, and 5 mM nAg-embedded PVP hydrogels were successfully prepared by γ-irradiation at 25, 35, and 45 kGy. The occurrence of surface plasmon spectra in the UV spectrum ~ 400 nm to 430 nm indicated that nAg was formed. Size and nAg distribution were investigated by TEM and SEM-EDX. The results demonstrated that the silver nanoparticles, with spherical shape of ~4 nm to 10 nm, were well distributed. Gamma irradiation at 25, 35, and 45 kGy scarcely affected the gel fraction and WVTR. The amount of cumulative release of Ag from the nAg-embedded PVP hydrogel in SBF at 37°C increased with an increase in Ag content. The 1 mM and 5 mM nAg-embedded PVP hydrogels showed antibacterial activity against pathogens. The higher the nAg content, the shorter the contact time to obtain 99% bacterial reduction rate. All of the hydrogels were confirmed to be non-toxic to L929 cells. The 5 mM nAg-embedded PVP hydrogels not only provided a clean, moist environment for wound healing, but also prevented bacterial infection most effectively and enhanced wound recovery.

3.7 Acknowledgements

The authors gratefully acknowledge the National Center of Excellence for Petroleum, Petrochemicals, and Advanced Materials; the Petroleum and Petrochemical College (PPC), Chulalongkorn University; and Department of Biotechnology, Faculty of Science, Ramkhamhaeng University, Thailand. Appreciation is also expressed to the Department of Veterinary Surgery, Faculty of Veterinary Science, Chulalongkorn University, Thailand.

3.8 Funding

This work was supported by the [Office of the Higher Education Commission, Thailand] under Grant [number 100/2550].

3.9 References

1. Deng, C.M., et al., *Biological properties of the chitosan-gelatin sponge wound dressing.* Carbohydrate Polymers, 2007. **69**(3): p. 583-589.
2. MacKay, D. and A.L. Miller, *Nutritional support for wound healing.* Altern Med Rev, 2003. **8**(4): p. 359-77.
3. Enoch, S. and D.J. Leaper, *Basic science of wound healing.* Surgery (Oxford), 2008. **26**(2): p. 31-37.
4. Stojadinovic, A., et al., *Topical advances in wound care.* Gynecol Oncol, 2008. **111**(2 Suppl): p. S70-80.
5. Darmstadt, G.L., *Antibiotics in the management of pediatric skin disease.* Dermatol Clin, 1998. **16**(3): p. 509-25.
6. Boateng, J.S., et al., *Wound healing dressings and drug delivery systems: a review.* J Pharm Sci, 2008. **97**(8): p. 2892-923.
7. Atiyeh, B.S., et al., *Effect of silver on burn wound infection control and healing: review of the literature.* Burns, 2007. **33**(2): p. 139-48.
8. Shrivastava, S., et al., *Characterization of enhanced antibacterial effects of novel silver nanoparticles.* Nanotechnology, 2007. **18**(22).
9. Rujitanaroj, P.O., N. Pimpha, and P. Supaphol, *Wound-dressing materials with antibacterial activity from electrospun gelatin fiber mats containing silver nanoparticles.* Polymer, 2008. **49**(21): p. 4723-4732.
10. Rattanaruengsrikul, V., N. Pimpha, and P. Supaphol, *Development of gelatin hydrogel pads as antibacterial wound dressings.* Macromol Biosci, 2009. **9**(10): p. 1004-15.
11. Eckhardt, S., et al., *Nanobio silver: its interactions with peptides and bacteria, and its uses in medicine.* Chem Rev, 2013. **113**(7): p. 4708-54.
12. Robert, W. and B. Robert, *Infection and the Chronic Wound: A Focus on Silver.* Advances in Skin & Wound Care, 2005. **18**: p. 2-12.
13. Popović, Z.K., et al., *On the Use of Radiation Technology for Nanoscale Engineering of Silver/Hydrogel Based Nanocomposites for Potential Biomedical Application.* The Open Conference Proceedings Journal, 2010. **1**: p. 200-206.

14. Thomas, V., et al., *A versatile strategy to fabricate hydrogel-silver nanocomposites and investigation of their antimicrobial activity.* J Colloid Interface Sci, 2007. **315**(1): p. 389-95.

15. Girard, J., et al., *Development of a polystyrene sulfonate/silver nanocomposite with self-healing properties for biomaterial applications.* Comptes Rendus Chimie, 2013. **16**(6): p. 550-556.

16. Nair, L.S. and C.T. Laurencin, *Silver nanoparticles: Synthesis and therapeutic applications.* Journal of Biomedical Nanotechnology, 2007. **3**(4): p. 301-316.

17. Wang, H.S., et al., *Preparation of silver nanoparticles by chemical reduction method.* Colloids and Surfaces a-Physicochemical and Engineering Aspects, 2005. **256**(2-3): p. 111-115.

18. He, C., et al., *Formation and characterization of silver nanoparticles in aqueous solution via ultrasonic irradiation.* Ultrason Sonochem, 2014. **21**(2): p. 542-8.

19. Perni, S., V. Hakala, and P. Prokopovich, *Biogenic synthesis of antimicrobial silver nanoparticles capped with l-cysteine.* Colloids and Surfaces A: Physicochemical and Engineering Aspects, 2013.

20. Raut, R.W., V.D. Mendhulkar, and S.B. Kashid, *Photosensitized synthesis of silver nanoparticles using Withania somnifera leaf powder and silver nitrate.* Journal of Photochemistry and Photobiology B: Biology, 2014. **132**: p. 45-55.

21. Song, C., et al., *Preparation, characterization, and antibacterial activity studies of silver-loaded poly(styrene-co-acrylic acid) nanocomposites.* Mater Sci Eng C Mater Biol Appl, 2014. **36**: p. 146-51.

22. Sun, Q., et al., *Green synthesis of silver nanoparticles using tea leaf extract and evaluation of their stability and antibacterial activity.* Colloids and Surfaces A: Physicochemical and Engineering Aspects, 2014. **444**: p. 226-231.

23. Wu, J., et al., *In situ synthesis of silver-nanoparticles/bacterial cellulose composites for slow-released antimicrobial wound dressing.* Carbohydr Polym, 2014. **102**: p. 762-71.

24. Zhao, X., et al., *Microwave-assisted synthesis of silver nanoparticles using sodium alginate and their antibacterial activity.* Colloids and Surfaces A: Physicochemical and Engineering Aspects, 2014. **444**: p. 180-188.

25. Rosiak, J.M. and P. Ulanski, *Synthesis of hydrogels by irradiation of polymers in aqueous solution.* Radiation Physics and Chemistry, 1999. **55**(2): p. 139-151.

26. Ghosh, K. and S.N. Maiti, *Mechanical properties of silver-powder-filled polypropylene composites.* Journal of Applied Polymer Science, 1996. **60**(3): p. 323-331.

27. Liu, M.H., et al., *An investigation of the interaction between polyvinylpyrrolidone and metal cations.* Reactive & Functional Polymers, 2000. **44**(1): p. 55-64.

28. Jin, R., et al., *Photoinduced conversion of silver nanospheres to nanoprisms.* Science, 2001. **294**(5548): p. 1901-3.

29. Shin, H.S., et al., *Mechanism of growth of colloidal silver nanoparticles stabilized by polyvinyl pyrrolidone in gamma-irradiated silver nitrate solution.* J Colloid Interface Sci, 2004. **274**(1): p. 89-94.

30. Suber, L., et al., *Preparation and the mechanisms of formation of silver particles of different morphologies in homogeneous solutions.* J Colloid Interface Sci, 2005. **288**(2): p. 489-95.

31. Rao, Y.N., et al., *Gamma irradiation route to synthesis of highly re-dispersible natural polymer capped silver nanoparticles.* Radiation Physics and Chemistry, 2010. **79**(12): p. 1240-1246.

32. Gasaymeh, S.S., et al., *Synthesis and Characterization of Silver/Polyvinilpirrolidone (Ag/PVP) Nanoparticles Using Gamma Irradiation Techniques.* American Journal of Applied Sciences, 2010. **7**(7): p. 879-888.

33. Ajji, Z., I. Othman, and J.M. Rosiak, *Production of hydrogel wound dressings using gamma radiation.* Nuclear Instruments & Methods in Physics Research Section B-Beam Interactions with Materials and Atoms, 2005. **229**(3-4): p. 375-380.

34. Spinks, J.W.T.W.R.J., *An introduction to radiation chemistry.* 1990, New York: Wiley.

35. Janata, E., A. Henglein, and B. Ershov, *First clusters of Ag+ ion reduction in aqueous solution.* The Journal of Physical Chemistry, 1994. **98**(42): p. 10888-10890.

36. Shameli, K., et al., *Green synthesis of silver/montmorillonite/chitosan bionanocomposites using the UV irradiation method and evaluation of antibacterial activity.* International journal of nanomedicine, 2010. **5**(1): p. 875-887.

37. Du, B.D., et al., *Preparation of colloidal silver nanoparticles in poly(N-vinylpyrrolidone) by gamma-irradiation.* Journal of Experimental Nanoscience, 2008. **3**(3): p. 207-213.

38. Savas, H. and O. Guven, *Gelation, swelling and water vapor permeability behavior of radiation synthesized poly(ethylene oxide) hydrogels.* Radiation Physics and Chemistry, 2002. **64**(1): p. 35-40.

39. Naznin, M., et al., *Influence of Acacia catechu Extracts and Urea and Gamma Irradiation on the Mechanical Properties of Starch/PVA-Based Material.* ISRN Polymer Science, 2012. **2012**: p. 1-8.

40. Sibbald, R.G., et al.., *Preparing the wound bed 2003: focus on infection and inflammation.* Ostomy Wound Manage, 2003. **49**(11): p. 24-51.

41. Wu, P., et al., *In vitro assessment of water vapour transmission of synthetic wound dressings.* Biomaterials, 1995. **16**(3): p. 171-5.